



Optics Letters

Photonic generation of tunable dual-chirp microwave waveforms using a dual-beam optically injected semiconductor laser

PEI ZHOU,¹  HAO CHEN,² NIANQIANG LI,^{1,*} RENHENG ZHANG,¹ AND SHILONG PAN² 

¹School of Optoelectronic Science and Engineering, Soochow University, Suzhou 215006, China

²Key Laboratory of Radar Imaging and Microwave Photonics, Ministry of Education, Nanjing University of Aeronautics and Astronautics, Nanjing 210016, China

*Corresponding author: nli@suda.edu.cn

Received 9 December 2019; revised 5 February 2020; accepted 6 February 2020; posted 6 February 2020 (Doc. ID 385527); published 4 March 2020

An approach to generating dual-chirp microwave waveforms (DCMWs) is proposed and experimentally demonstrated. The proposed scheme consists of a typical semiconductor slave laser (SL), which is subject to a dual-beam optical injection from two master lasers with one being positively detuned (ML_1) and the other negatively detuned (ML_2) from the SL. Under proper injection conditions, the SL operates in the so-called Scenario B of dual-beam injection. After optical-to-electrical conversion, a dual-frequency microwave signal can be generated with one of its two frequencies increasing linearly and the other decreasing linearly as the ML_1 injection strength is increased. By incorporating a fast injection strength controller (formed by an intensity modulator and an electrical control signal), a DCMW with a large time-bandwidth product can be generated. In the experimental demonstration, a DCMW with a temporal period of 1 μ s has been obtained. This simultaneously offers an up-chirp (13.4–20.2 GHz) and a down-chirp (27.3–20.5 GHz), and its frequency tunability has been achieved by simply adjusting the injection parameters. Furthermore, the auto-ambiguity function of the generated DCMW has also been investigated, which proves that the proposed scheme has the ability to improve the range-velocity resolution and, thus, could be promising for use in radar systems. © 2020 Optical Society of America

<https://doi.org/10.1364/OL.385527>

Thanks to the pulse compression technique, wideband chirped microwave waveforms, phase-coded waveforms, or time-frequency coded waveforms can achieve both a large detection range and a high range resolution in radar systems [1]. A linearly chirped microwave waveform (LCMW) has been considered as one of the most commonly used radar waveforms, since its time-bandwidth product (TBWP) can be very large. An LCMW, however, has severe delay-Doppler coupling due to its knife-edge type ambiguity function, which might cause a poor two-dimensional united resolution of range and velocity [1]. To cope with this challenge, dual-chirp microwave waveforms

(DCMWs) have been introduced [2]. A DCMW consists of two complementary chirped components within the same temporal period, i.e., one is up-chirped, and the other is down-chirped. With the help of the information of the arrival time of the two complementary chirped components, the unwanted delay-Doppler coupling effect in an LCMW could be overcome. With a thumbtack-like ambiguity function, a DCMW is very promising in reducing the delay-Doppler coupling and improving the range-velocity resolution [3].

In general, the DCMW generation by purely electrical techniques suffers from limited frequency and bandwidth. Therefore, many photonic-based approaches have been proposed to generate these waveforms with high carrier frequencies and large bandwidths [3–7]. One major method relies on a baseband single-chirp waveform, as well as a nested electro-optic modulator, such as a dual-parallel Mach-Zehnder modulator (MZM) [3,4] or a dual-polarization MZM [5]. In these methods, the baseband single-chirp waveform and a microwave carrier are applied to a sub-MZM of the nested electro-optic modulator. Apart from an integrated nested modulator, two cascaded MZMs can also be used for DCMW generation [6]. The main drawback is its high cost and complex structure, which usually requires a wideband microwave arbitrary waveform generator (AWG) and a high-speed modulator. Another method is based on a Fourier domain mode-locked optoelectronic oscillator (OEO) [7]. By matching the sweep period of the output frequency with the round-trip time of the OEO cavity, Fourier domain mode locking can be established. However, the generated DCMW has a poor linearity and a limited bandwidth of less than 4 GHz. Recently, photonic generation of microwave signals based on optically injected semiconductor lasers operating in the period-one (P1) oscillation state has received considerable attention [8–15]. By properly varying the injection parameters, the P1 frequency can be tuned from a few to over 100 GHz [8]. Up to now, P1 oscillations have been applied for generating tunable microwave signals [9,10], optical pulses [11], microwave frequency combs [12], triangular pulses [13], and frequency-hopping sequences [14]. In our prior work [15], we proposed and experimentally demonstrated a scheme

to generate LCMWs with a large TBWP by simply controlling the injection strength.

In this Letter, the generation of interesting DCMWs is presented by incorporating a typical semiconductor slave laser (SL), which is subject to a dual-beam optical injection from two master lasers with one being positively detuned (ML_1) and the other negatively detuned (ML_2) from the SL. Under proper injection conditions, the SL operates in the so-called Scenario B of dual-beam injection [16]. Specifically, the P1 oscillation excited by the first-beam injection is preserved, while that of the second-beam injection is suppressed. Following the optical-to-electrical conversion, a dual-frequency microwave signal can be generated with its two frequencies increasing and decreasing with the increment of the ML_1 injection strength. By taking advantage of the fast injection strength controlling technique, tunable DCMWs with a large TBWP can be obtained. In the proof-of-concept experiment, a DCMW with a temporal period of 1 μ s has been obtained, which simultaneously offers an up-chirp (13.4–20.2 GHz) and a down-chirp (27.3–20.5 GHz). Additionally, the frequency tunability and auto-ambiguity function of the generated DCMW have also been investigated.

Figure 1 depicts the experimental setup used for the DCMW generation. A commercial distributed-feedback semiconductor laser (Actech LD15DM) is applied as the SL. Under a bias current of 31.7 mA and a stabilized temperature of 24.2°C, the free-running frequency and power of the SL are 194.19 THz and 3.63 dBm, respectively. Two optical carriers (ML_1 and ML_2) from a multi-channel laser source (Agilent N7714A) are optically injected into the SL, which are detuned by f_1 and f_2 from the free-running frequency of the SL. A tunable optical attenuator (Att) and a polarization controller (PC) are included after ML_1 and ML_2 to control their optical injection power and polarization. A fast injection strength controller (FISC) has also been incorporated, which contains a 10 Gb/s MZM and an electrical control signal $S(t)$ from a 120 MHz AWG (Agilent 81150A). Afterwards, the light of both MLs is combined through a 50/50 coupler and is then injected into the SL through an optical circulator (CIR). At the third port of the CIR, a 90/10 optical coupler is inserted to tap 10% of the signal power for measurement in an optical spectral analyzer (OSA, Yokogawa AQ6370C) with a 0.02 nm resolution. The other 90% of the SL output is sent to a 30 GHz photodetector (PD) for optical-to-electrical conversion. Then the electrical properties of the generated microwave signal are analyzed in an 80 GSa/s real-time oscilloscope (OSC, Keysight DSO-X

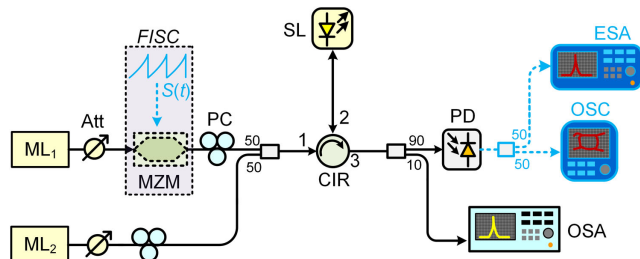


Fig. 1. Experimental setup of the proposed DCMW generator. ML, master laser; Att, tunable optical attenuator; PC, polarization controller; FISC, fast injection strength controller; MZM, Mach–Zehnder modulator; $S(t)$, control signal; CIR, optical circulator; SL, slave laser; PD, photodetector; OSA, optical spectral analyzer; ESA, electrical spectral analyzer; OSC, oscilloscope.

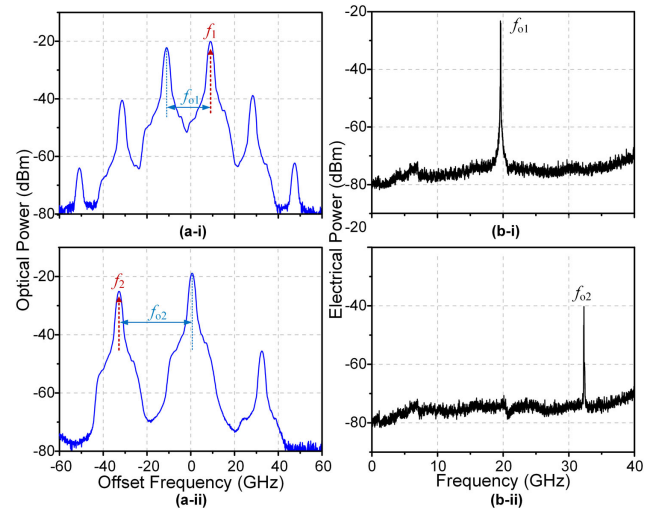


Fig. 2. (a) Optical and (b) electrical spectra of the SL subject to single-beam injection. (i) f_1 single-beam injection and (ii) f_2 single-beam injection.

92504A) and a 40 GHz electrical spectral analyzer (ESA, R&S FSV 40). Throughout this Letter, the resolution bandwidth of the ESA is fixed at 3 MHz.

First, the electrical control $S(t)$ is not applied, and the injection strength is varied by adjusting the tunable optical attenuator. The frequency detuning and injection strength of ML_1 (f_1, ξ_1) are set to be (9.1 GHz, 0.55). In this Letter, the injection strength is defined as the square root of the power ratio between the injected optical signal and output of the free-running SL. Under these circumstances, a P1 oscillation state is excited with a fundamental frequency of $f_{01} = 19.3$ GHz. The optical and electrical spectra of the SL subject to single-beam injection from ML_1 are illustrated in Figs. 2(a-i) and 2(b-i), respectively. As can be seen in Fig. 2(a-i), two highly dominant frequency components, i.e., a regenerated optical carrier and a redshifted cavity mode, separated by the P1 oscillation of f_{01} , are observed after optical injection. Throughout this Letter, the x axis of the optical spectrum is relative to the free-running frequency of the SL. The corresponding electrical spectrum of the generated 19.3 GHz signal is presented in Fig. 2(b-i). In contrast to ML_1 , ML_2 has a negative frequency detuning from the SL. In this case, another P1 oscillation with $f_{02} = 32.3$ GHz is also induced by the single-beam injection of $(f_2, \xi_2) = (-32.8$ GHz, 0.49). Figures 2(a-ii) and 2(b-ii) present the resultant optical and electrical spectra, respectively, for the sole ML_2 injection. In Fig. 2(a-ii), the optical spectrum also contains two dominant frequency components. At the output of the PD, a 32.3 GHz microwave signal is measured in Fig. 2(b-ii).

When both beams are simultaneously injected, the SL operates in the so-called Scenario B of dual-beam injection according to Ref. [16], where the nonlinear dynamic state by f_1 single-beam injection is preserved while that of f_2 single-beam injection is suppressed. As can be observed in the optical spectrum of Fig. 3(a), the system output is dominated by the P1 oscillation originating from f_1 single-beam injection; however, f_2 injection beam could modify the f_1 injection induced dynamics through nonlinear mixing. The final output spectrum is the result of nearly degenerate four-wave mixing

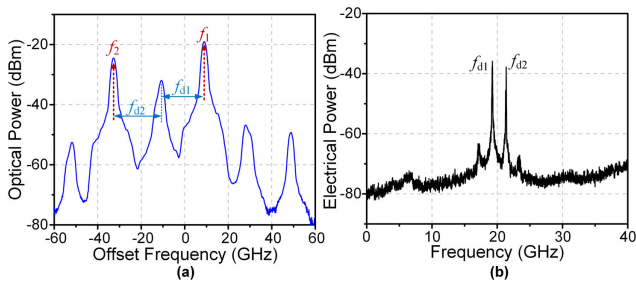


Fig. 3. (a) Optical and (b) electrical spectra of the SL subject to dual-beam injection.

(NDFWM) between f_2 and its nearest line in f_1 -injection induced P1 oscillation. The main components are regenerated optical carriers (f_1 , f_2) and the shifted cavity mode. At the output of the PD, two major frequency components (f_{d1} , f_{d2}) = (19.3 GHz, 21.3 GHz) are found in the electrical spectrum of Fig. 3(b), which indicates that a dual-frequency microwave signal is obtained. The two new frequencies meet the conditions of $f_{d1} \approx f_{o1}$ and $f_{d2} \approx f_1 - f_2 - f_{d1}$. Note here that in Fig. 3(b) the frequency component of $f_1 - f_2 = 41.9$ GHz has been blocked due to the limited bandwidth of the PD used in the experiment.

It has been proved that for a fixed master-slave detuning, the P1 oscillation frequency would increase approximately linearly with the injection strength [8]. Thus, when both positive f_1 and negative f_2 are fixed, frequencies of the generated dual-frequency microwave signal (f_{d1} , f_{d2}) will increase and decrease monotonously with the ML_1 injection strength ξ_1 , respectively. Typical results of this phenomenon are displayed in Fig. 4(a), which are consistent with our expectation. In this process, the injection strength ξ_1 is changed by tuning the ML_1 injection power through a tunable optical attenuator. Figure 4(b) shows superimposed optical spectra of the SL under different ML_1 injection strengths ξ_1 . The optical spectra are corresponding to the circumstances of (i), (ii), (iii), and (iv) in Fig. 4(a). One can observe that frequencies of the regenerated optical carriers (f_1 , f_2) are fixed, while that of the cavity mode decreases or redshifts with increasing ξ_1 . The results further confirm that frequencies of the dual-frequency signal would linearly increase and decrease with the increasing ML_1 injection strength, respectively.

Then, in order to generate DCMWs, the FISC is enabled. By setting the control signal $S(t)$ with a quasi-sawtooth profile, the ML_1 injection strength ξ_1 would increase linearly in a temporal period. The resultant instantaneous frequencies of f_{d1} and f_{d2} would correspondingly increase and decrease linearly. In other

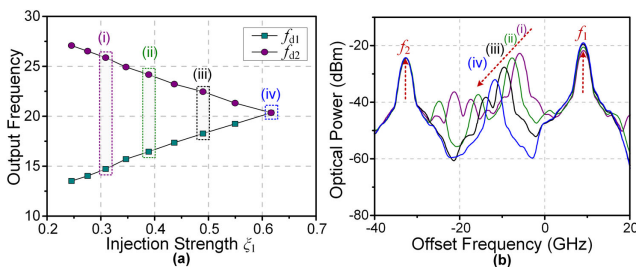


Fig. 4. (a) Frequencies of the generated dual-frequency microwave signal as a function of ML_1 injection strength and (b) superimposed optical spectra of the SL under different ML_1 injection strengths.

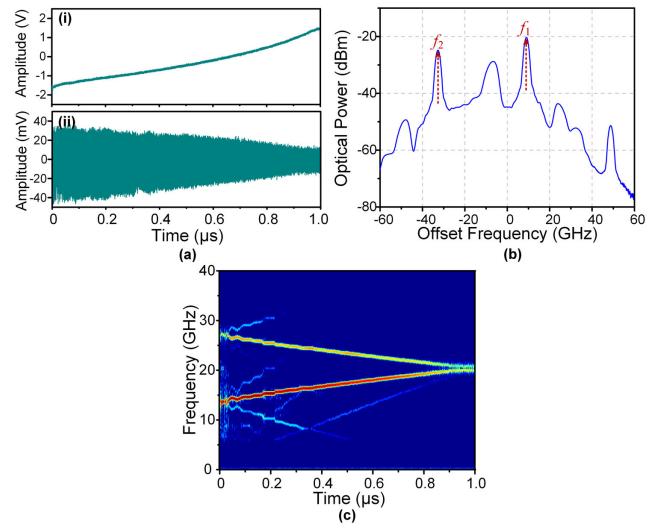


Fig. 5. (a) Measured waveforms of (i) the control signal and (ii) the generated DCMW with one period; (b) optical spectrum of the SL; and (c) instantaneous frequency-time diagram.

words, a DCMW has been generated. The detuning frequencies (f_1 , f_2) are kept to (9.1, -32.8 GHz). As plotted in Fig. 5(a-i), a 1 MHz control signal with an amplitude of 3.2 V is applied to the MZM to control the injection strength. Here the profile of $S(t)$ is mainly designed to compensate for the nonlinearity of the amplitude transfer function of the system [15]. As a consequence, a DCMW with a temporal period of 1 μ s is produced, and its temporal waveform is shown in Fig. 5(a-ii). The uneven amplitude of the generated DCMW is mainly caused by the dynamic competition between the injection-shifted cavity mode and the regenerated optical carriers under a temporally varying injection strength. This problem can be solved by using either electrical or optical power limiting techniques [17]. In Fig. 5(b), the measured optical spectrum of the generated DCMW is plotted. Figure 5(c) shows the instantaneous frequency-time diagram for the generated DCMW at the output of PD in Fig. 1. The instantaneous frequency-time diagram is obtained by applying a 3.2 ns sliding Hamming window for a short-time Fourier transformation on the temporal waveform [18]. As can be seen, the generated waveform contains both an up-chirp (13.4–20.2 GHz) and a down-chirp (27.3–20.5 GHz) waveform in the same 1 μ s period. The TBWP of the generated DCMW is calculated to be 13600. Some weak spurs can also be observed, which are mainly caused by the beat-notes between the unwanted optical components, e.g., high-order optical sidebands and four-wave mixing components.

The frequency tunability of DCMWs is of great importance for any application and could be achieved by adjusting the detuning frequencies and injection strengths of both MLs, as long as the SL is kept in the Scenario B of a dual-beam optically injected semiconductor laser, and the output spectrum is the result of NDFWM between f_2 and its nearest line in f_1 -injection induced P1 oscillation. For instance, Fig. 6 provides instantaneous frequency-time diagrams of the generated DCMWs with different values of the frequency coverage. In Fig. 6(a), the generated signal has a frequency coverage of (25.5–28.0 GHz) and (17.2–14.7 GHz) in the 1 μ s period. In Fig. 6(b), the frequency range has been moved to (25.8–30.0 GHz) and (25.8–21.6 GHz).

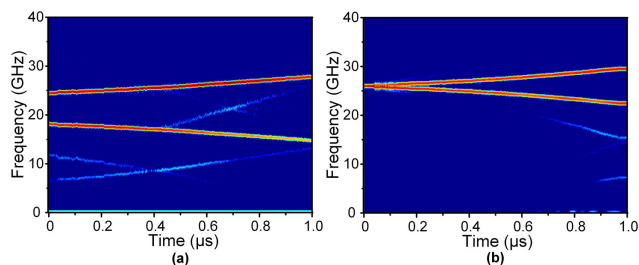


Fig. 6. Instantaneous frequency-time diagrams of the generated DCMWs with different values of the frequency coverage.

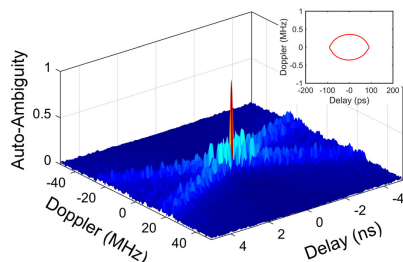


Fig. 7. Auto-ambiguity function of the generated DCMW. Inset: the -3 dB contour map.

In order to evaluate the delay-Doppler coupling characteristics of the radar transmitting waveform, the auto-ambiguity function is introduced [1]. This function measures the compression of a microwave waveform both in time and frequency domain, corresponding to range and Doppler, respectively. To further show the performance characteristic of the generated DCMWs, the auto-ambiguity function is calculated offline. The case shown in Fig. 6(b) is taken as an example for the estimation of the auto-ambiguity function. The result is shown in Fig. 7, and it is interesting to find a thumbtack-like auto-ambiguity function, which is different from a knife-edge shape for the case of a conventional LCMW. This means that the microwave waveform generated by the proposed scheme exhibits better performance, i.e., a reduced delay-Doppler coupling and improved range-velocity resolution. Specifically, according to the -3 dB contour map shown in the inset, the main lobe of the auto-ambiguity function has a full-width at half-maximum (FWHM) of ~ 175 ps in delay and ~ 0.72 MHz in Doppler.

It should be noticed that heterodyning the single-beam optically injected SL with a separate standalone laser is an alternative approach to generating DCMWs. This is, however, different from the proposed dual-beam injection approach, where there exist competitions between two single-beam injection dynamics, and the output optical frequency components could affect each other through the charge carriers in the laser cavity [16]. Additionally, the investigation of microwave linewidths based on the two approaches is important, and it is of interest to take into account some possible linewidth-narrowing methods,

such as using an optoelectronic feedback structure [10] or two phase-coherent optical carriers acting as the master lasers. This topic will be deeply discussed and demonstrated elsewhere.

In conclusion, we have proposed and demonstrated an approach to generating DCMWs based on a dual-beam optically injected semiconductor laser. To the best of our knowledge, this is the first demonstration of the DCMW generation using the nonlinear dynamics of dual-beam injection. Tunable DCMWs with a large TBWP can be generated by simply controlling the injection strength. In the experimental demonstration, a DCMW with a temporal period of $1 \mu\text{s}$ has been obtained, which simultaneously offers an up-chirp and a down-chirp with a bandwidth of up to 6.8 GHz, corresponding to a TBWP as large as 13600 . The frequency tunability of the generated waveform has been realized by simply adjusting the frequency detuning and injection strength. Additionally, the auto-ambiguity function of the generated DCMW has also been calculated, and the result confirms the good performance of the proposed technique. Without using any high-speed modulator or AWG, the proposed technique features a low-cost, simple structure and, thus, may find wide applications in radar systems.

Funding. Startup Funding of Soochow University (GJ15900119, GJ15900519, Q415900119).

Disclosures. The authors declare no conflicts of interest.

REFERENCES

1. M. Skolnik, *Radar Handbook*, 3rd ed. (McGraw-Hill, 2008).
2. A. Amar and Y. Buchris, *IEEE Signal Process. Lett.* **21**, 1078 (2014).
3. D. Zhu and J. Yao, *IEEE Photonics Technol. Lett.* **27**, 1410 (2015).
4. K. Zhang, S. H. Zhao, A. J. Wen, W. Zhang, W. L. Zhai, T. Lin, and X. Li, *Opt. Lett.* **44**, 4004 (2019).
5. S. Zhu, M. Li, N. H. Zhu, and W. Li, *Opt. Lett.* **43**, 2466 (2018).
6. Y. X. Xu, T. Jin, H. Chi, S. L. Zheng, X. F. Jin, and X. M. Zhang, *IEEE Photonics Technol. Lett.* **29**, 1253 (2017).
7. T. Hao, J. Tang, N. Shi, W. Li, N. Zhu, and M. Li, *Opt. Lett.* **44**, 1912 (2019).
8. S. C. Chan, S. K. Hwang, and J. M. Liu, *Opt. Lett.* **31**, 2254 (2006).
9. N. G. Usechak, J. S. Suelzer, and J. W. Haefner, *IEEE Photonics Technol. Lett.* **29**, 1132 (2017).
10. J. S. Suelzer, T. B. Simpson, P. Devgan, and N. G. Usechak, *Opt. Lett.* **42**, 3181 (2017).
11. P. Zhou, F. Zhang, B. Gao, and S. Pan, *IEEE Photonics Technol. Lett.* **28**, 1827 (2016).
12. X. Q. Xu, L. Fan, G. Q. Xia, and Z. M. Wu, *IEEE Access* **6**, 55284 (2018).
13. P. Zhou, F. Zhang, Q. Guo, and S. Pan, *IEEE Photonics Technol. Lett.* **30**, 1317 (2018).
14. P. Zhou, F. Zhang, X. Ye, Q. Guo, and S. Pan, *IEEE Photonics J.* **8**, 5501909 (2016).
15. P. Zhou, F. Zhang, Q. Guo, and S. Pan, *Opt. Express* **24**, 18460 (2016).
16. X. Q. Qi and J. M. Liu, *IEEE J. Quantum Electron.* **47**, 762 (2011).
17. J. W. Shi, F. M. Kuo, N. W. Chen, S. Y. Set, C. B. Huang, and J. E. Bowers, *IEEE Photonics J.* **4**, 215 (2012).
18. N. Kehtarnavaz, *Digital Signal Processing System Design*, 2nd ed. (Academic, 2008).